

5-3-2016

Fbxo30 Regulates Mammopoiesis by Targeting the Bipolar Mitotic Kinesin Eg5.

Yan Liu

George Washington University

Yin Wang

Zhanwen Du

Xiaoli Yan

Pan Zheng

See next page for additional authors

Follow this and additional works at: http://hsrc.himmelfarb.gwu.edu/smhs_peds_facpubs

 Part of the [Amino Acids, Peptides, and Proteins Commons](#), [Cell Biology Commons](#), and the [Pediatrics Commons](#)

APA Citation

Liu, Y., Wang, Y., Du, Z., Yan, X., Zheng, P., & Liu, Y. (2016). Fbxo30 Regulates Mammopoiesis by Targeting the Bipolar Mitotic Kinesin Eg5. *Cell Reports*, 15 (5). <http://dx.doi.org/10.1016/j.celrep.2016.03.083>

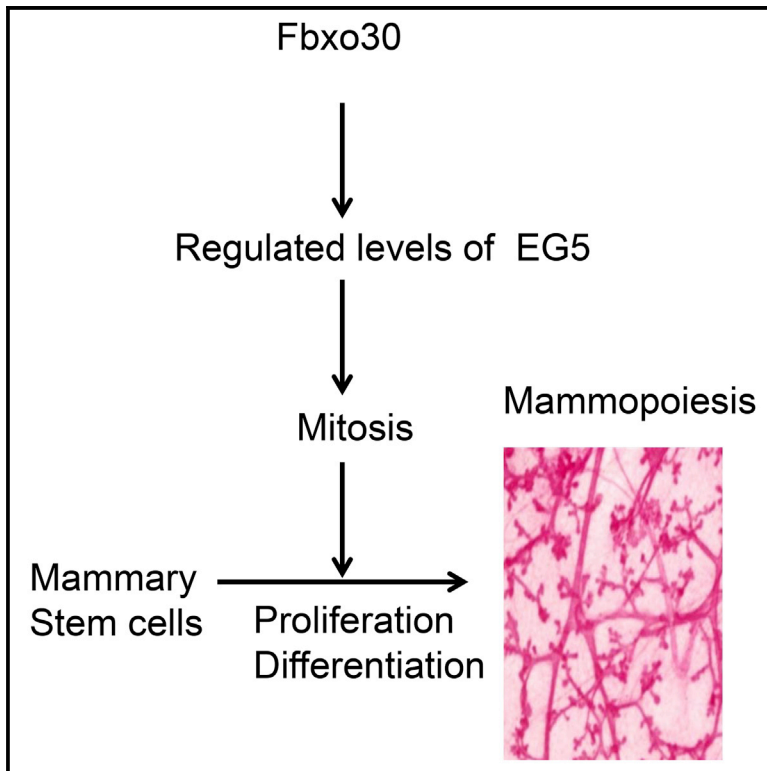
This Journal Article is brought to you for free and open access by the Pediatrics at Health Sciences Research Commons. It has been accepted for inclusion in Pediatrics Faculty Publications by an authorized administrator of Health Sciences Research Commons. For more information, please contact hsrc@gwu.edu.

Authors

Yan Liu, Yin Wang, Zhanwen Du, Xiaoli Yan, Pan Zheng, and Yang Liu

***Fbxo30* Regulates Mammopoiesis by Targeting the Bipolar Mitotic Kinesin Eg5**

Graphical Abstract



Authors

Yan Liu, Yin Wang, Zhanwen Du, Xiaoli Yan, Pan Zheng, Yang Liu

Correspondence

ywang@cnmc.org (Y.W.),
panz@cnmc.org (P.Z.),
yaliu@cnmc.org (Y.L.)

In Brief

Liu et al. identify *Fbxo30* as the E3 ligase for bipolar mitotic kinesin Eg5. Deletion or shRNA silencing of *Fbxo30* increases Eg5 and disrupts mitosis, while germline deletion of *Fbxo30* disrupts normal mammopoiesis.

Highlights

- *Fbxo30* is identified as the E3 ligase for bipolar mitotic kinesin Eg5
- Deletion or shRNA silencing of *Fbxo30* increases Eg5 and disrupts mitosis
- Germline deletion of *Fbxo30* disrupts normal mammopoiesis



Fbxo30 Regulates Mammopoiesis by Targeting the Bipolar Mitotic Kinesin Eg5

Yan Liu,^{1,3} Yin Wang,^{1,3,*} Zhanwen Du,² Xiaoli Yan,² Pan Zheng,^{1,*} and Yang Liu^{1,*}¹Center for Cancer and Immunology Research, Children's Research Institute, Children's National Medical Center, Washington, DC 20010, USA²Key Laboratory for Infection and Immunity, Institute of Biophysics, Chinese Academy of Science, Beijing 100101, China³Co-first author*Correspondence: ywang@cnmc.org (Y.W.), panz@cnmc.org (P.Z.), yaliu@cnmc.org (Y.L.)<http://dx.doi.org/10.1016/j.celrep.2016.03.083>

SUMMARY

Fbxo30 is an orphan member of the F-box protein family with no known substrate or function. Here we report that, while *Fbxo30*^{-/-} mice exhibit normal development, growth, lifespan, and fertility, the females fail to nurture their offspring as a result of defective mammopoiesis. Mass spectrometry analysis of Fbxo30-associated proteins revealed that Fbxo30 specifically interacts with the bipolar spindle kinesin EG5 (encoded by *Kif11*). As a result, Fbxo30 targets Eg5 for ubiquitinylation and controls its oscillation during the cell cycle. Correlated with EG5 dysregulation, *Fbxo30*^{-/-} mammary epithelial cells exhibit multiple defects in centrosome homeostasis, mitotic spindle formation, and proliferation. Effects on proliferation, centrosome homeostasis, and mammopoiesis in the *Fbxo30*^{-/-} mice were rescued through normalization of Eg5 activity using shRNA and/or an EG5 inhibitor. Our data reveal the Fbxo30-Eg5 interaction as a critical checkpoint in mammopoiesis and a critical role for ubiquitinylation-regulated Eg5 oscillation in the cell cycle.

INTRODUCTION

F-box proteins (FBXs) are defined by the shared protein-protein interaction domain called F-box. Based on the existence of additional structural motifs, FBXs are divided into three subfamilies, including FBXW (for the WD40 domain), FBXL (for leucine-rich motif), and FBXO (for other motifs) (Jin et al., 2004). FBXs often interact with a specific motif on the substrate called degron. Since the interactions between the best-characterized FBXs and their substrates are regulated by phosphorylation of the degron (Köivomägi et al., 2011; Liu et al., 2002; Nash et al., 2001; Wei et al., 2005), the term phosphodegron was coined to epitomize regulation between FBXs and their substrates (Skaar et al., 2013). However, it is increasingly clear that many FBX-substrate interactions are either based on recognition of the unmodified degron sequence (D'Angiolella et al., 2010, 2012) or recognition of degron with other covalent modification, such as glycosylation

(Yoshida et al., 2002). More recently, phosphorylation of degron has been shown to inhibit FBXL12 binding to p85β subunit of PI3K (Kuchay et al., 2013).

The biological function of FBX is informed by their specific substrates. By conferring substrate specificity to the SCF ubiquitin E3 ligases, FBXs regulate a variety of cellular functions, including the cell cycle (Carrano et al., 1999; Frescas and Pagano, 2008), signal transduction (Köivomägi et al., 2011; Kuchay et al., 2013; Liu et al., 2002; Nash et al., 2001; Wei et al., 2005), DNA repair (D'Angiolella et al., 2012), and genomic instability (Puklowski et al., 2011), among others (Skaar et al., 2013). Despite the extensive effort, the substrates for the majority of FBXs remain to be identified. This gap prevents us from fully understanding the function and mechanism of action of FBX. Identification of the substrates for the orphan FBX is a major focus in cell biology, as these efforts not only clarify the function of the orphan FBXs but also elucidate, to our knowledge, novel cellular regulatory pathways.

FBXO30 is an orphan FBX with no known substrates. Here, we take a reverse genetic approach to evaluate the function of Fbxo30 in mice. Our data revealed an unexpected function of the Fbxo30 gene in mammopoiesis, including branch morphogenesis and defective production of mature luminal epithelial cells. Mass spectrometry analysis of Fbxo30-associated proteins revealed motor protein Eg5 as Fbxo30 substrate. By regulating Eg5 abundance, Fbxo30 regulates mitosis and mammopoiesis. Our data not only revealed an unexpected function of Fbxo30 in organogenesis but also identified it as a critical regulator for mitosis.

With identification of mammary stem cells (Shackleton et al., 2006; Stingl et al., 2006), the mouse has emerged as a major tool to study mammopoiesis. Accumulating data led to a developmental pathway for differentiation of mammary stem cells into progenitors for basal myoepithelial and luminal epithelial cells, respectively (Shackleton et al., 2006; Stingl et al., 2006; Visvader, 2009; Visvader and Stingl, 2014). Genetic studies indicate critical roles for Slug and Sox9 as key determinants of mammary stem cell function (Guo et al., 2012). Commitment to a luminal fate versus a basal fate is influenced by the expression of p63 and Notch 1 and Notch 3, respectively (Bouras et al., 2008; Raouf et al., 2008; Yalcin-Ozuysal et al., 2010). Elf5 has emerged as a key in specifying luminal fate (Chakrabarti et al., 2012; Oakes et al., 2008), while GATA3 directs differentiation to luminal

epithelial cells (Asselin-Labat et al., 2007). Our data presented herein reveal a critical role for Fbxo30-EG5 interaction mammary gland morphogenesis and, thus, suggest a critical checkpoint in mammapoiesis.

RESULTS

Mice with Targeted Mutations of *Fbxo30* Reveal a Critical Role for Fbxo30 in Mouse Mammapoiesis

With the exception of a small stretch of 68 amino acids (aa) encoded by exon 3, the majority of the 746 aa of Fbxo30 are encoded by exon 2. We replaced the 3.5 kb genomic DNA encompassing the entire region of exon 2 (2.1 kb) and part of intron 2 (1.4 kb) with an in-frame GFP cDNA followed by a Neomycin cassette for selection (Figure S1). The heterozygous mutant embryonic stem cells (ESCs) of C57BL/6 origin were used to generate chimeric mice. The null allele was germline-transmitted at a Mendelian ratio, suggesting that the *Fbxo30* gene was not essential for mouse development. Moreover, *Fbxo30*^{-/-} and *Fbxo30*^{+/+} littermates had normal fertility and grew at a similar rate with indistinguishable lifespan. Surprisingly, regardless of the paternal genotypes, mutation of the *Fbxo30* in the nursing female reduced the survival of the offspring, as the survival rates of offspring from *Fbxo30*^{-/-}, *Fbxo30*^{+/-}, and *Fbxo30*^{+/+} females were 0%–12%, 55%–69%, and 82%–84%, respectively (Table S1). Only a small number of offspring were successfully nurtured by *Fbxo30*^{-/-} mice, usually after multiple pregnancies.

Since the offspring of *Fbxo30*^{-/-} females developed normally with foster mothers and since necropsy revealed that the pups died of starvation (data not shown), we examined the mammary glands by histology and flow cytometry. In mammary gland whole mounts, virgin *Fbxo30*^{-/-} mice had atrophic mammary glands, characterized by both reduced branching and atrophic large ducts (images in Figure 1A). The ratio between lateral branches and large ducts was decreased by *Fbxo30* deletion (Figure 1A, right panel). Pregnancy of wild-type (WT) mice is associated with increased branching and formation of alveolar structures in the branches. However, the *Fbxo30*^{-/-} mammary glands showed diminished branching with the alveoli forming adjacent to the large ducts (Figure 1B). Histological analysis revealed that, while WT mammary glands had proliferated massively at day 2 postpartum, those in *Fbxo30*^{-/-} mice remained largely atrophic (Figure 4C). Furthermore, while most of the glandules in *Fbxo30*^{+/+} mice were filled with milk droplets, very few glandules in the *Fbxo30*^{-/-} mice contained milk droplets. These findings explained why the *Fbxo30*^{-/-} female failed to nurture the offspring.

To identify the relative number of luminal epithelial versus myoepithelial cells, we stained mammary sections with antibodies specific for cytokeratin (CK) 8 (luminal epithelial cells) or CK5 (basal myoepithelial cells). A reduction in the ratio of CK8⁺/CK5⁺ cells was observed in the *Fbxo30*^{-/-} mammary glands (Figure 1D). The normal development of myoepithelial cells was confirmed by using a panel of different markers, including CK14, CK17, and α SMA (Figure 1E). Remarkably, production of mucin by the luminal epithelial cells was largely abrogated by *Fbxo30* deletion (Figure 1E).

We analyzed the cellular composition of the mammary glands using CD29, CD49f, CD61, and CD24 markers (Visvader, 2009). CD45 and CD31 were used to mark hematopoietic cells and vascular endothelial cells, respectively, for exclusion. We used flow cytometry to characterize the frequency of major cell types in the mammary gland. Representative fluorescence-activated cell sorting (FACS) profiles are shown in Figure 2A, while summary data of the major mammary gland cell types are shown in Figures 2B and 2C. Among the CD45⁻CD31⁻ cells, we observed a reduction in the proportion of CD24⁺CD29^{lo} cells (Figure 2A, upper panels). Since essentially all of the CD24⁺CD29^{lo} cells expressed high levels of CD49f (Figure 2A, lower panels), they belonged to luminal epithelial cells. Conversely, the percentage of CD24⁺CD29^{hi}CD49⁺ myoepithelial cells was increased (Figure 2A). In combination, the increase of myoepithelial and decrease of luminal epithelial cells resulted in a nearly 2-fold decrease in the relative abundance of luminal lineages (Figure 2B). Correspondingly, the absolute numbers of luminal epithelial cells recovered from the *Fbxo30*^{-/-} was more severely reduced (Figure 2C).

We used the accepted CD31⁻CD45⁻CD24^{hi}CD29^{hi}Sca1⁻ markers to assess the amounts of mammary stem cells in WT and *Fbxo30*^{-/-} mice. Among CD45⁻CD31⁻ cells from mammary glands, a reduction of the CD24^{hi}CD29^{hi} cells was observed in the *Fbxo30*^{-/-} mammary gland, as demonstrated in Figure 3A (left panels). However, the CD49^{hi}Sca1⁻ populations were reduced in the *Fbxo30*^{-/-} mammary gland. As a result, the percentage of CD31⁻CD45⁻CD24^{hi}CD29^{hi}Sca1⁻ mammary stem cells was unaffected. Therefore, *Fbxo30* mutation does not affect the number of mammary stem cells (Figure 3B). Despite their normal numbers, the size of the *Fbxo30*^{-/-} mammosphere was markedly reduced (Figures 3C and 3D).

Taken together, the data in Figures 1, 2, and 3 reveal that, while *Fbxo30* is not required for mammary stem cell maintenance, it is required for differentiation and/or expansion of luminal progenitors into ductal and/or alveolar cells.

Fbxo30 Is the E3 Ligase of EG5

Fbxo30 is an orphan FBX with no known substrate. To fill in this gap, we isolated the FLAG-tagged Fbxo30-associated proteins by coimmunoprecipitation (coIP) with anti-FLAG antibodies. The proteins eluted with free FLAG peptides were digested with trypsin and analyzed by mass spectrometry. In addition to those from Fbxo30, peptides from Skp1 and Cullin were prominently represented, as expected. Interestingly, to our knowledge, seven unique peptides from the bipolar kinesin motor protein EG5 were identified (Figure 4A). To confirm this interaction, we probed anti-FLAG immunoprecipitates of either vector or Fbxo30-FLAG-transfected 293T cells. As shown in Figure 4B, anti-FLAG specifically co-precipitated EG5, Skp1, and Cul1. Since there are no commercial antibodies that satisfactorily immunoprecipitate FBXO30, we knocked in a 3× FLAG tag immediately before the stop codon in the *FBXO30* open reading frame (Zhang et al., 2008) (Figure S2), and we used an anti-FLAG mAb to determine whether endogenous FBXO30 associates with EG5. As shown in Figure 4C (left panel), anti-FLAG precipitated FBXO30 and EG5 as well as polyubiquitinated proteins. Reciprocally, anti-EG5 specifically co-precipitated FBXO30 (Figure 4C,

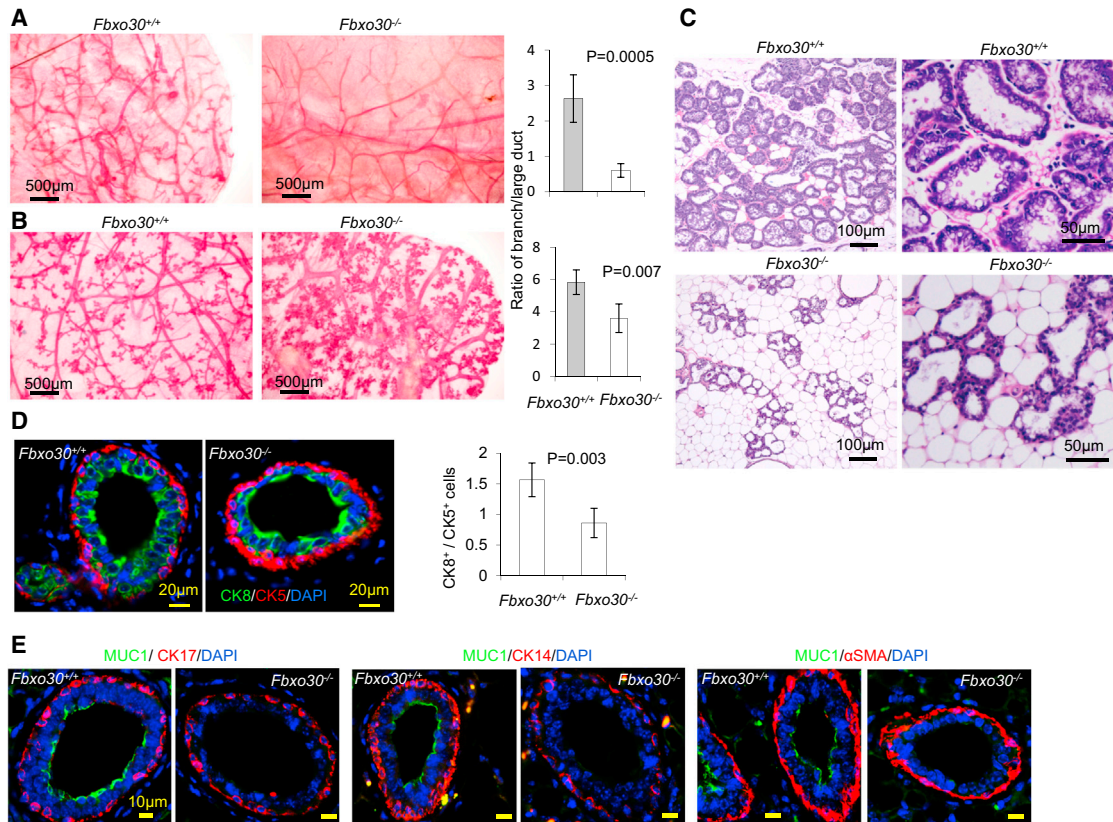


Figure 1. Defective Mammapoiesis in *Fbxo30*^{-/-} Mice

(A) Morphological defects of virgin *Fbxo30*^{-/-} mammary glands by whole-mount Carmine alum staining show reduced branching and atrophic large ducts. The images are representative from three independent experiments, each of which involves three mice per group. Bar graphs depict ratios of length of lateral branches to that of the large ducts. Length was measured by NeuroLucida Tracing software (MBF Bioscience). Data shown are means and SEM ($p = 0.0005$). Data presented are summary data from one experiment involving three mice per group. One fat pad per mouse was analyzed. The data have been reproduced in another independent experiment.

(B) Morphological defects of mammary glands in 12-day pregnant *Fbxo30*^{-/-} mice and WT littermates were visualized in whole-mount sections. Reduction in mammary gland branching in pregnant *Fbxo30*^{-/-} female mice was determined as in (A), except that the mammary glands were isolated from day 12 of the first pregnancy ($p = 0.007$). Data presented are summary data from one experiment involving three mice per group. One fat pad per mouse was analyzed. The data have been reproduced in another independent experiment.

(C) Histology analysis of postpartum mammary gland reveals atrophy and lack of milk droplets in the *Fbxo30*^{-/-} female mammary glands. Samples collected at day 2 postpartum were fixed in formalin and stained with H&E. Similar results were obtained in eight mice analyzed (three WT and five *Fbxo30*^{-/-} mice).

(D) Reduction of luminal epithelial cells in the *Fbxo30*^{-/-} mammary gland. Formalin-fixed mammary gland tissue sections were stained with antibodies specific for either cytokeratin 5 (CK5, basal myoepithelial cells) or cytokeratin 8 (CK8, luminal epithelial cells). The images in the upper panels are representative of four independent experiments involving one mouse per group (scale bar, 20 μ m). Data shown in the right panel are the ratios of CK8⁺/CK5⁺ cells. The error bar depicts the SEM ($n = 10$ glands from one fatpad in each group). Data have been reproduced three times.

(E) Defective production of musin by luminal epithelial cells in *Fbxo30*^{-/-} mammary glands. As in (D), except that the mammary sections were stained with antibodies against CK14, SMA, and CK17, respectively, in conjunction with Muc1.

right panel). These results confirmed the endogenous association between EG5 and FBXO30. Moreover, inhibition of proteasome increased EG5 in whole-cell lysate (Figure 4D). Using truncation mutant of Eg5, we observed that Fbxo30 interacts with the C-terminal region rather than the N-terminal and central parts of Eg5. The binding sites likely reside between aa 812 and 1,052 (Figure 4E).

To confirm that Fbxo30 is the E3 ligase for EG5, we isolated the Fbxo30 proteins from Fbxo30-FLAG transfectants and incubated them with Myc-tagged EG5 in the ubiquitinylation reaction mixture containing an E1 ubiquitin-activating enzyme and an E2

ubiquitin-conjugating enzyme. The extent of Eg5 ubiquitinylation was determined by immunoblot with an anti-polyubiquitin antibody. As shown in Figure 4F (upper panel), incubation of EG5 with Fbxo30 in the presence of E1 and E2 resulted in robust EG5 ubiquitinylation. After normalizing the amount of input protein, it was clear that EG5 ubiquitinylation did not require phosphorylation at either T927 or S1040, two phosphorylation sites critical for the regulation of EG5 activity by CDK1 and Plk1-NEK9-NEK6/7, respectively (Bertran et al., 2011; Blangy et al., 1995; Rapley et al., 2008), as the relative amounts of polyubiquitinated EG5 increased even though the amounts of EG5 were

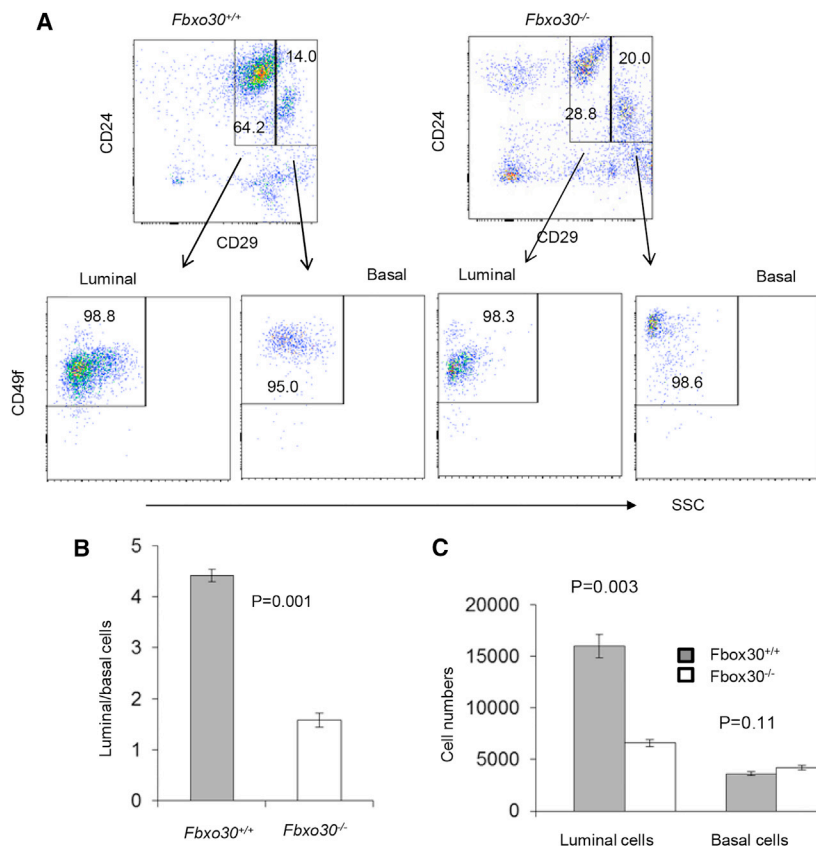


Figure 2. Fbxo30 Deficiency Affects Luminal versus Basal Lineage Choice

(A) Representative FACS profiles depicting selective reduction in luminal epithelial cells in the mammary gland of the *Fbxo30*^{-/-} mice. The markers and gating strategy used to define specific mammary gland cell types are indicated. (B) Reduction in luminal/basal ratio among *Fbxo30*^{-/-} mammary epithelial cells is shown. (C) Number of recoverable luminal and basal epithelial cells in mammary gland per mice. Data shown are the numbers of epithelial cells with either luminal or basal epithelial cell markers based on FACS staining. Data shown in this figure are representative data from an experiment involving three mice in each group and have been reproduced three times.

reduced. The mechanism of reduced accumulation of mutant EG5 remains to be explained.

To identify potential ubiquitylation sites, we focused on a patch of Lysine (K) between aa 891 and 913. As shown in Figure 4F (lower panel), while mutations of K891R and K899R substantially reduced polyubiquitylation of Eg5, other mutations had minimal effect. These data further support ubiquitylation of Eg5 by Fbxo30, although they do not necessarily rule out additional ubiquitylation sites on Eg5.

Eg5 activities are tightly regulated during the cell cycle by phosphorylation (Bertran et al., 2011; Blangy et al., 1995; Rapley et al., 2008). Since it is unclear whether Eg5 oscillates during cell cycle, we arrested, at G0/1, S, and M phases, the HCT116 cells expressing a FLAG-tagged FBXO30 under the control of its endogenous promoter. As shown in Figure 5A, EG5 levels increased progressively from G0/1 phase, to S phase, to M phase but reduced after the cells were released from the M phase arrest. The peak EG5 level at M phase correlated with the lowest FBXO30 level. To test whether Fbxo30 is responsible for Eg5 accumulation, we arrested WT and *Fbxo30*^{-/-} mouse embryonic fibroblasts (MEFs) at G1/G0, S, and M phases and compared the Eg5 levels. As shown in Figure 5B, Eg5 levels increased from G1 phase to S phase but peaked at the M phase in the WT MEF. Targeted mutation of *Fbxo30* accelerated the increase of Eg5, as it peaked at S phase rather than M phase. Since Fbxo30 was expressed at lower levels at M phase, it was expected that deletion of this gene would not significantly

affect EG5 levels (Figure 5B). The mechanism for fluctuations of Fbxo30 during cell cycles is currently unknown.

To determine whether Fbxo30 regulates Eg5 in mammary gland epithelial (MGE) cells, we arrested WT and *Fbxo30*^{-/-} MGE cells at S phase, and we determined Eg5 accumulation using immunofluorescence in conjunction with DAPI (Figure 5C). S-phase-synchronized *Fbxo30*^{-/-} MGE cells exhibited markedly increased overall Eg5 levels, as reflected by huge increases of Eg5⁺ spots. Despite comparable mRNA levels of the *Kif11* gene, which encodes EG5 (Figure 5D), freshly isolated MGE cells had substantially elevated Eg5 protein, as revealed by western blot (Figure 5E). To determine whether Fbxo30 regulates Eg5 in vivo, we compared the cellular levels of Eg5 in mammary glands from WT and *Fbxo30*^{-/-} mice by immunofluorescence. This analysis revealed a marked increase in the cellular concentration of EG5 in *Fbxo30*^{-/-} mammary gland (Figure 5F).

As an ATPase motor protein, Eg5 is targeted to the mitotic spindle and centrosome and plays a critical role in mitosis (Mardin and Schiebel, 2012; Nigg and Stearns, 2011). Consistent with the abnormal levels of Eg5 in *Fbxo30*^{-/-} MGE cells (Figure 5), the proliferation rate of *Fbxo30*^{-/-} MGE cells also was markedly reduced over three passages (Figure 6A). To determine whether the defective proliferation in MGE cells is attributable to increased Eg5 activity, we used small hairpin RNA (shRNA) to silence the *Kif11* gene in the *Fbxo30*^{-/-} MGE cells (Figure 6B, right panel). Consistent with a critical role for Eg5 in cell proliferation (Bertran et al., 2011; Blangy et al., 1995; Rapley et al., 2008), growth of WT MGE cells was inhibited by shRNA specific for the *Kif11* gene. In contrast, shRNA silencing of *Kif11* increased the proliferation of *Fbxo30*^{-/-} MGE cells (Figure 6B). Furthermore, *Kif11* shRNA significantly increased the size of mammospheres (Figure 6C).

Reintroduction of WT Fbxo30 to the mammary epithelial cells through ectopic expression partially restored the mammosphere formation (Figure 6D). While these data confirmed the

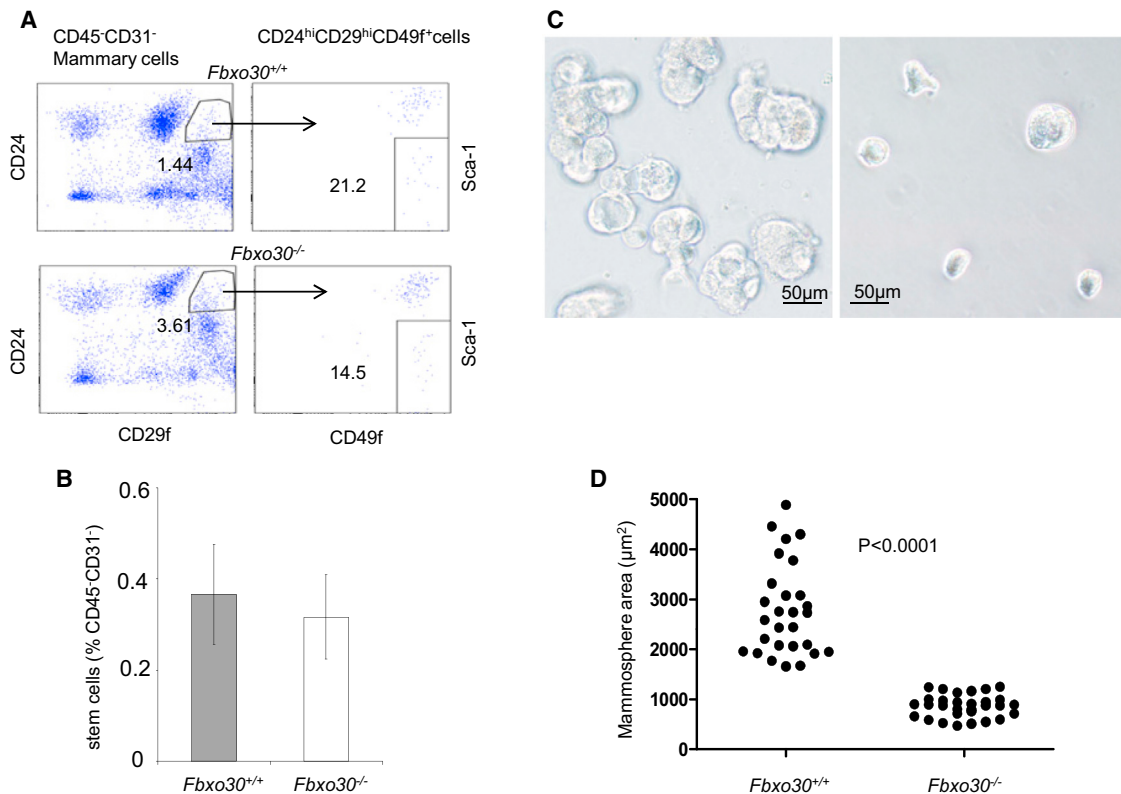


Figure 3. Impact of Fbxo30 Deficiency on Number and Differentiation of Mammary Stem Cells

(A) Representative FACS profiles depicting WT and *Fbxo30*^{-/-} mammary epithelial cells. The stem cells were defined as CD29^{hi}CD49f^{hi}CD24^{hi}Sca-1⁻. (B) Summary data on the percentage of mammary stem cells in WT and *Fbxo30*^{-/-} mammary gland. Data shown are means and SEM (n = 5 mice per group), summarized from three independent experiments. (C) *Fbxo30*^{-/-} stem cells have diminished production of progeny in mammosphere culture. Representative images depict the reduction in mammosphere size (scale bar, 50 μm). (D) Areas of the representative mammosphere. Each dot represents the area of an individual sphere, as calculated using Scion software. These data have been reproduced three times.

function of *Fbxo30*, they also suggested that ectopic expression of *Fbxo30* does not fully recapitulate the function of endogenous alleles.

To determine whether increased Eg5 is responsible for the defective mammapoiesis during pregnancy, we treated day 6 pregnant *Fbxo30*^{-/-} mice with the Eg5 inhibitor monastrol (Mayer et al., 1999), and we analyzed the mammary gland morphology at day 12. As shown in Figures 6E and 6F, a short-term treatment of the *Fbxo30*^{-/-} mice with monastrol substantially rescued mammapoiesis, as revealed by the increased branching and distance between the alveoli and the large ducts. Therefore, elevated Eg5 activity is responsible for the defective mammapoiesis of *Fbxo30*^{-/-} MGE cells in both virgin and pregnant mice.

Given the role of Eg5 in centrosome separation (Mardin et al., 2011; Mardin and Schiebel, 2012), we evaluated the impact of *Fbxo30* mutation on mitosis. Based on DNA content, it was clear that deletion of *Fbxo30* caused G2/M arrest and polyploidy (Figure 7A). To understand how *Fbxo30* defects affect genome instability and G2/M arrest, we analyzed Eg5 distribution and mitotic spindles in mitotic WT MGE cells. We found

that Eg5 was targeted to bipolar mitotic spindles, with a higher concentration at the two poles of the MGE cells. However, in the *Fbxo30*^{-/-} MGE cells, Eg5 was targeted to multipolar spindles or bipolar multiple spindles, resulting in abnormal separation of chromosomes (Figures 7B and 7C). This was due to overactive Eg5, as the number of cells with abnormal spindles was normalized by Eg5 inhibitor (Figure 7D). Consistent with increased multipolar spindles, targeted mutation caused centrosome amplification, as indicated by the percentage of MGE cells with more than two centrosomes (Figure 7E). This was mediated by increased Eg5, as the reduction of Eg5 through shRNA silencing of *Kif11* attenuated the defects (Figure 7F).

A critical issue is whether defective spindle formation can be found to increase in the *Fbxo30*^{-/-} mammary glands. To address this issue, we stained mammary gland with anti-β-tubulin antibodies and DAPI and searched for cells with mitotic spindle in mammary glands. Mitotic cells were readily observed in the mammary glands from the *Fbxo30*^{-/-} mice but rarely in those from WT mice, which is consistent with a G2/M arrest of *Fbxo30*^{-/-} MGE cells in vivo. Remarkably, while the WT MGE

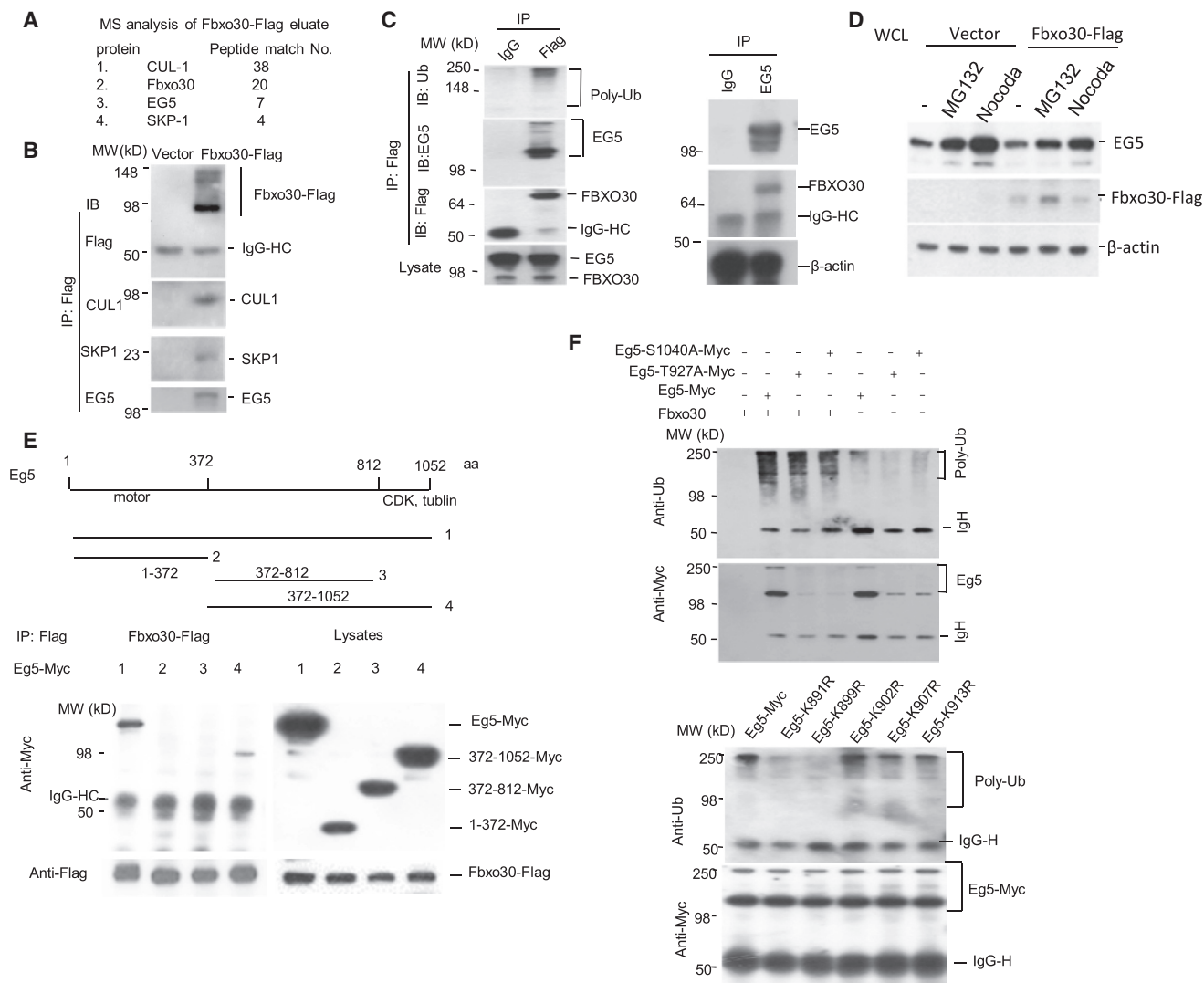


Figure 4. Fbxo30 Is an E3 Ligase for EG5

(A) Identification of EG5 and other SCF components in a complex by mass spectrometry analysis. 293T cells were transfected with cDNA encoding FLAG-tagged Fbxo30 or an unrelated protein (Laforin). FLAG-tagged proteins were purified by immunoprecipitating with anti-FLAG. Immunoprecipitated proteins were eluted with FLAG peptide. The Fbxo30-associated proteins were concentrated by SDS-PAGE. The gel slices of ~1 cm were submitted to Taplin Biological Mass Spectrometry Facility at the Harvard Medical School (<https://taplin.med.harvard.edu>) for using the microcapillary liquid chromatography-tandem mass spectrometry (LC-MS/MS) technique. The numbers of unique, to our knowledge, peptides associated with Fbxo30 are listed, while peptides shared with Laforin are excluded.

(B) Confirmation of EG5-SCF complex by coIP. cDNA encoding FLAG-tagged Fbxo30 was transfected into 293T cells. After immunoprecipitation with anti-FLAG, the precipitates were probed for EG5, SKP1, and CUL1 by their specific antibodies.

(C) Association between endogenous EG5 and Fbxo30. The endogenous FBXO30 was tagged with a 3 \times FLAG epitope by homologous knockin (see Figure S2). The left panel shows that anti-FLAG-Fbxo30 co-precipitated endogenous EG5; the right panel shows co-precipitation of endogenous FBXO30 by anti-EG5.

(D) Impact of proteasome inhibitor MG132 and M phase arrest on endogenous EG5 levels: effect of ectopically expressed Fbxo30. After 24 hr of being transfected with empty vector or Fbxo30-FLAG-expressing vector, the 293T cells were treated with 2.5 μ M MG132 or 50 nM nocodazole for an additional 6 hr before being lysed for western blot. Note that, in vector control, EG5 levels increased after MG132 treatment and that EG5 overexpression decreased EG5 at M phase.

(E) Eg5 C-terminal region interacts with Fbxo30. As in (B), except either full-length or indicated truncation mutants were used and that Eg5 was detected by anti-Myc antibody. The left panel shows the immunoprecipitation-western blot data, while the right panel depicts the expression levels in the lysates.

(F) In vitro ubiquitylation of Eg5 by Fbxo30. Data in upper panels show phosphorylation-independent ubiquitylation, while those in the lower panels show selectivity of ubiquitylation. Fbxo30-FLAG protein was purified from HEK293 cells transfected with FLAG-tagged Fbxo30 and incubated with bead-bound EG5 isolated from EG5-Myc-transfected cells and with a ubiquitylation system containing E1, E2, and proteasomal components. After removing the unbound components by re-immunoprecipitating Eg5 with a c-Myc antibody, the extent of Eg5 ubiquitylation was determined by immunoblot with an anti-polyubiquitin antibody (top), while the amount of EG5 was determined with an anti-Myc antibody (bottom). WT Eg5 was used in the upper panel, while the K > R mutants were compared with WT Eg5 in the lower panel. Data in (B)–(E) are representative images and have been repeated two times.

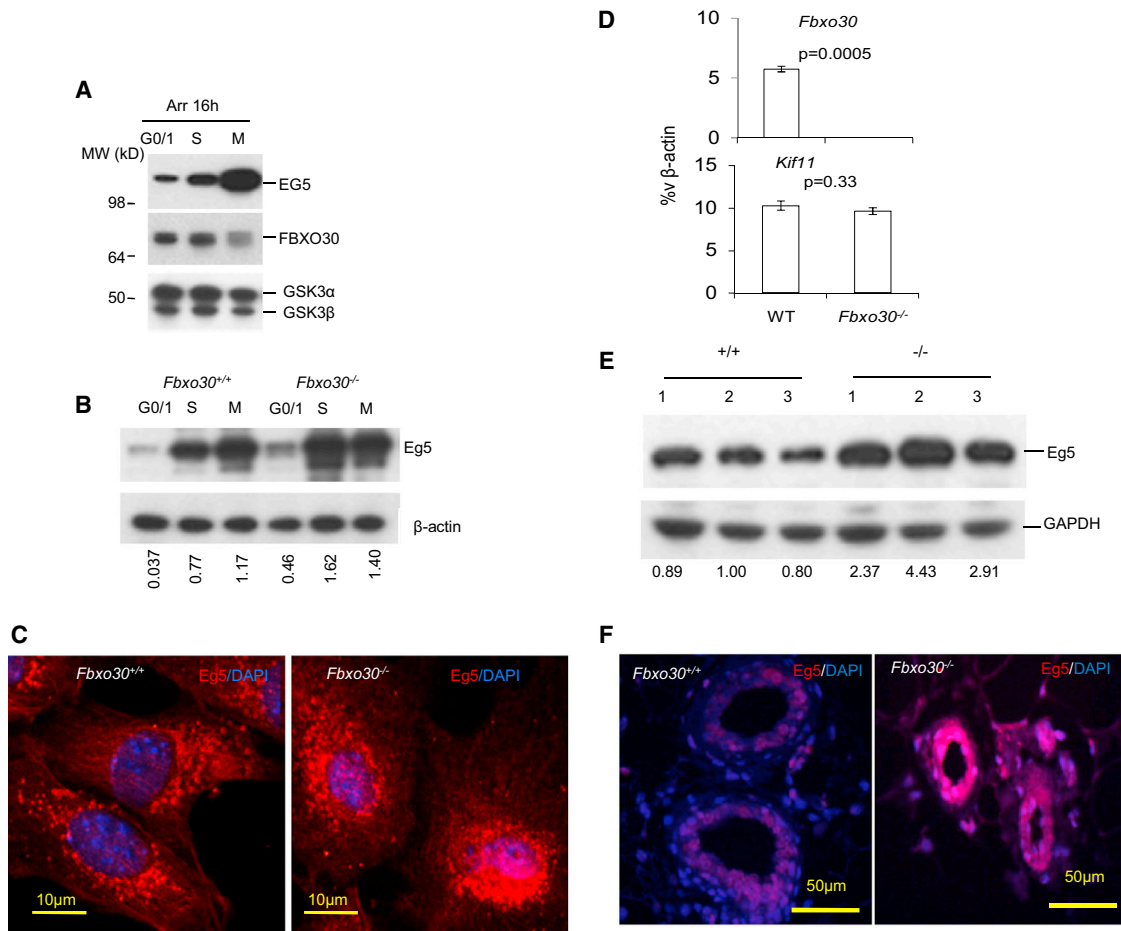


Figure 5. FBXO30 Regulates EG5 Oscillation during Cell Cycle

(A) Increased EG5 protein levels at mitosis correlate with reduced Fbxo30. HCT116 cells with Fbxo30-3x-FLAG knockin alleles were arrested at G0/1 phase with serum-free medium, early S phase with 1 μ g/ml aphidicolin, or M phase with 50 ng/ml nocodazole. All treatments were performed for 16 hr. The lysates were analyzed for the endogenous levels of EG5 and Fbxo30 by western blot. GSK3 levels were used as a loading control. Data shown have been reproduced three times.

(B) *Fbxo30* deletion greatly increases Eg5 levels at S and M phases of the *Fbxo30*^{-/-} MEFs. WT and *Fbxo30*^{-/-} MEFs were arrested for 16 hr in serum-free media, 1 μ g/ml aphidicolin, or 50 ng/ml nocodazole. The lysates were analyzed for the endogenous levels of EG5 by western blot. β -actin levels were used as a loading control. The relative amounts of EG5 protein are provided underneath each lane. The numbers indicate the ratio of signals from anti-EG5 over anti- β -actin. Data shown have been reproduced three times.

(C) Elevated Eg5 levels in *Fbxo30*^{-/-} MGE cells. WT and *Fbxo30*^{-/-} MGE cells were arrested at S phase with 1 μ g/ml aphidicolin for 16 hr. Images shown are representative of those obtained from three independent experiments.

(D) Normal expression of the *Kif11*(Eg5-encoding) gene in *Fbxo30*^{-/-} mammary glands. RNA isolated from single-cell suspension of WT and *Fbxo30*^{-/-} mammary glands was analyzed for expression of *Fbxo30* and *Kif11*. While deletion of *Fbxo30* abolished expression of *Fbxo30*, it had no effect on the *Kif11* transcript, as determined by real-time PCR.

(E) Western blot data using lysate MGE cells (n = 3). The images of the western blot are shown in the top panel. The relative amounts of Eg5 protein are provided underneath each lane. The numbers indicate the ratio of signals from anti-Eg5 over anti-Gapdh. These data have been reproduced twice.

(F) Eg5 staining in WT and *Fbxo30*^{-/-} mammary glands as determined by immunofluorescence. The nuclei are visualized by the DNA dye DAPI. Data shown are representative images from three experiments, each involving one fatpad from one mouse per group.

cells had normal bipolar mitotic spindle, essentially all of the mitotic cells in the *Fbxo30*^{-/-} mammary glands contained abnormal spindles, including those with mono- or multipolar spindles with abnormal donut-type chromatin (Figure 7G; Figure S3). The increase of cells with either mono- or multipolar spindles in mammary glands phenocopied what was observed in MEFs cultured from transgenic mice that overexpressed Eg5 (Castillo et al., 2007).

DISCUSSION

Taken together, we have demonstrated that Fbxo30 is an E3 ligase that specifically ubiquitinylates and regulates Eg5 levels in mammary epithelial cells and MEFs. The Fbxo30-Eg5 pathway controls centrosome homeostasis and genome stability. Since cells with abnormal mitotic spindles undergo apoptosis (Ganem et al., 2009), the defective cell growth and

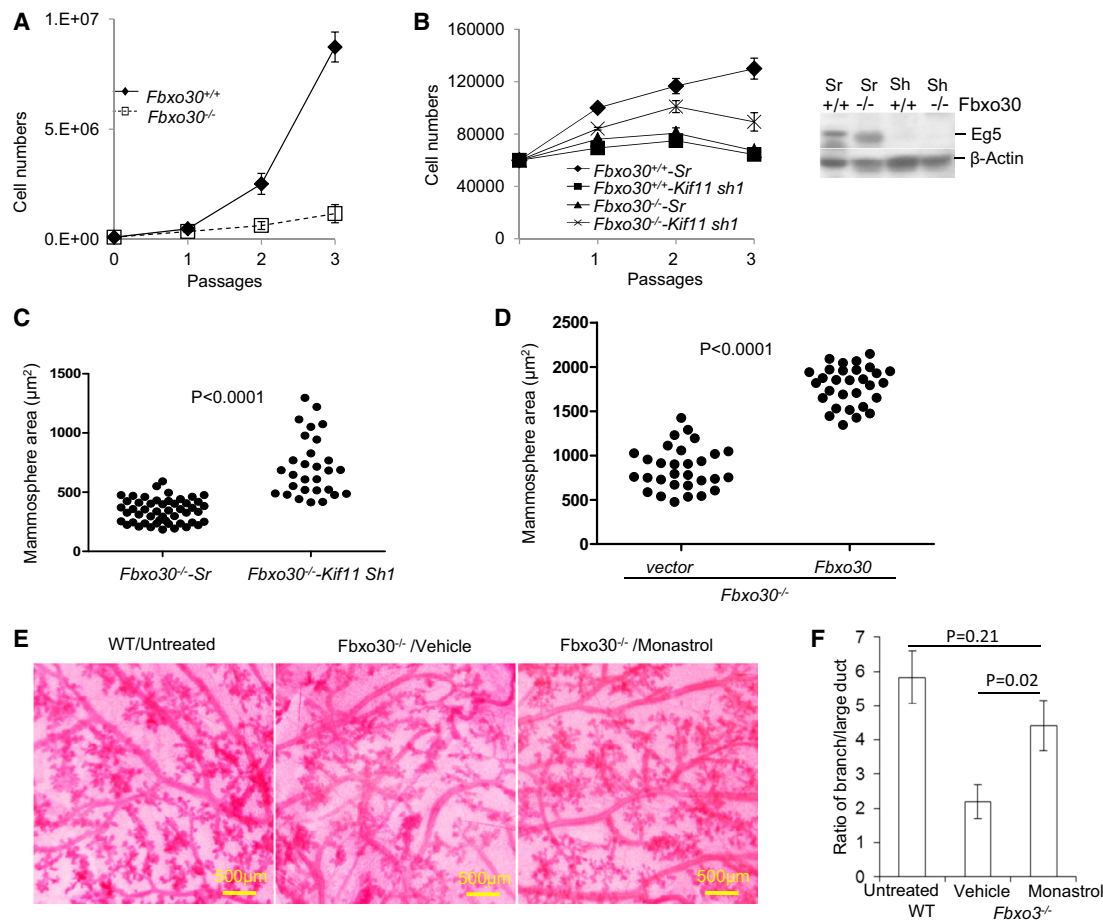


Figure 6. Fbxo30 Regulates Cell Proliferation and Mammapoiesis through EG5

(A) Fbxo30 is required for propagation of mammary epithelial cells in vitro. Data shown are the number of WT and *Fbxo30*^{-/-} MGE cells over three passages. (B) The shRNA silencing of *Kif11* reduces proliferation of WT MGE cells, but modestly enhances proliferation of *Fbxo30*^{-/-} MGE cells. Freshly isolated WT or *Fbxo30*^{-/-} MGE cells were transduced with lentiviral vectors with either scrambled or *Kif11* shRNA for 24 hr. Equal numbers of transduced cells were re-plated and counted over three passages. The efficiency of *Kif11* shRNA silencing is shown in the right panel. (C) The shRNA silencing of *Kif11* in *Fbxo30*^{-/-} MGE cells increases the size of mammospheres. Transduced primary MGE cells were cultured for mammosphere assay. Data shown are the surface area of individual spheres from the two groups. The p value was calculated by Student's t test. Data shown in (A)–(C) are representative of three independent cultures. (D) Ectopic expression of Fbxo30 partially restores sizes of *Fbxo30*^{-/-} mammospheres. *Fbxo30*^{-/-} epithelial cells were transduced with lentiviral vector alone or those with *Fbxo30* cDNA prior to culture. These data have been reproduced three times. (E and F) Restoration of mammapoiesis of pregnant *Fbxo30*^{-/-} mice by monastrol, including increased secondary branching and reduced alveoli associated with the large ducts. Day 6 pregnant *Fbxo30*^{-/-} mice received three injections of either vehicle control or monastrol (5 mg/kg, every other day, intraperitoneal injection) over a 6-day period. Mammary glands were harvested on day 12 of pregnancy and used for whole-mount sections. (E) Representative images of whole-mount sections from one of three mice in each group, one fatpad analyzed per mouse. This experiment has been repeated two times. A whole-mount section of WT mammary gland is included for comparison. (F) Summary data of the ratio of the length of lateral branches to that of the large ducts, as measured by NeuroLucida Tracing software. Data shown are from one of two independent experiments (n = 3 mice per group, one fat pad per mouse is analyzed). Error bars are SEM.

genome instability observed in the *Fbxo30*^{-/-} cells are intrinsically connected.

Previous studies have demonstrated that EG5 targeting to the spindle pole is regulated by phosphorylation at sites T927 and S1040 by Cdk1 and Plk1-Ned6, respectively (Bertran et al., 2011; Blangy et al., 1995; Rapley et al., 2008), and their phosphorylation is critical for correct formation of mitotic spindle. Our data demonstrate that phosphorylation of neither site is required for EG5 ubiquitinylation. Thus, Eg5 is subject to at least two layers

of regulation: Cdk1- and Plk1-Nek9-Nek6/7-mediated phosphorylation, which regulates localization but not Eg5 levels, and the Fbxo30-mediated ubiquitinylation, which controls Eg5 levels. A phospho-peptide analysis revealed that endogenous Eg5 was phosphorylated only at the T927 and S1040 sites in vivo (Rapley et al., 2008), and since mutation of neither site abolished Eg5 ubiquitinylation, it is likely that Fbxo30-mediated Eg5 degradation occurs either by a phosphorylation-independent pathway, which would be similar to the Fbxo1-CP110 and Fbxo11-BCL6

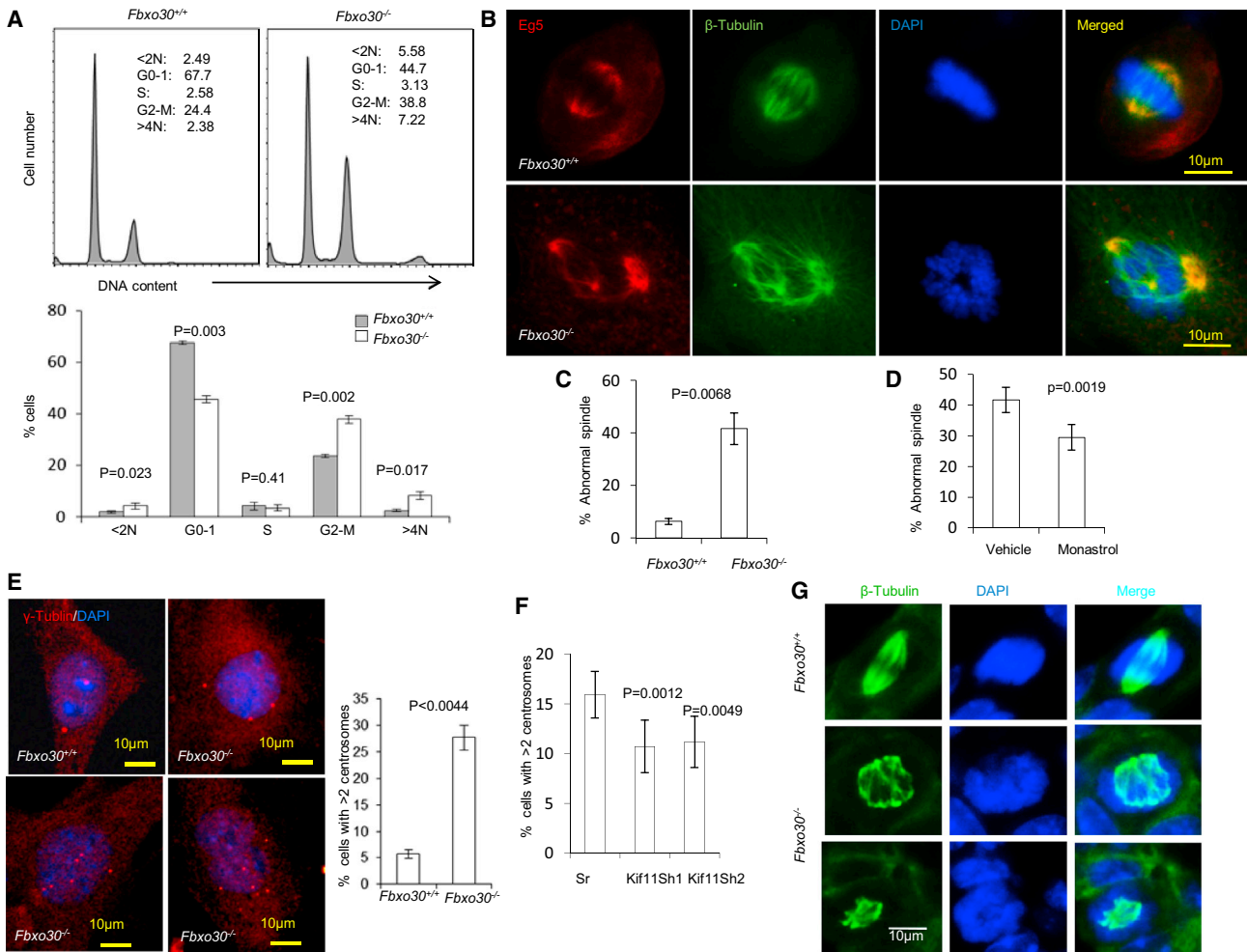


Figure 7. *Fbxo30* Deletion Causes Chromosomal Instability and Spindle Defects In Vivo and In Vitro

(A) DNA content analysis based on propidium iodide staining of ethanol-fixed MGE cells after two passages in vitro. Representative FACS profiles are shown on top and the summary data involving three mouse samples per group are shown on the bottom. Note a major increase in cells with >4N in DNA content.

(B) Deletion of *Fbxo30* causes formation of multipolar mitotic spindles. WT (upper panels) and *Fbxo30^{-/-}* (lower panels) MGE cells were stained for EG5, tubulin, and DNA.

(C) Summary data for three different cultures (n = 3) are shown.

(D) Monastrol treatment reduces the percentage of MGE cells with abnormal spindles. As in (C), except that the MGE cells prepared from *Fbxo30^{-/-}* mice were treated with either vehicle control or monastrol (30 nM) for 48 hr prior to staining.

(E) *Fbxo30* deletion causes abnormal centrosome amplification. The images on the left depict γ -tubulin distribution in a WT and three *Fbxo30^{-/-}* MGE cells, while the right panel shows the mean and SEM of the percentage of cells with more than two centrosomes (n = 15) and has been repeated three times.

(F) The shRNA silencing of the *Kif11* gene restores centrosome homeostasis in *Fbxo30^{-/-}* MGE cells. *Fbxo30^{-/-}* MGE cells were cultured in the presence of either vehicle or a low dose of monastrol (30 nM) for 48 hr. The centrosome number was determined by γ -tubulin staining. Data shown are means and SEM of the percentage of cells with more than two centrosomes (n = 10) and have been repeated three times.

(G) Accumulation of multipolar spindle mitotic cells in the *Fbxo30^{-/-}* mammary glands, as revealed by staining with anti- β -tubulin mAb and DAPI staining of frozen mammary gland sections. The top panels show a cell with a normal bipolar spindle in WT mammary gland; the lower panels show a cell in *Fbxo30^{-/-}* mammary gland with multipolar mitotic spindle and abnormal distribution of chromatin. Cells with mitotic spindle are difficult to find in vivo. Only one such cell was found in five slides prepared from five virgin mice, while more than 50 cells with mitotic spindle were found in two of the five slides from the five virgin *Fbxo30^{-/-}* mice. None of the mitotic spindles have normal morphology. Seven such cells are shown in Figure S3.

interactions (D'Angiolella et al., 2010; Duan et al., 2012), or by phosphorylation at other sites. Two recent studies demonstrated that the APC/C-CDH1 complex also caused ubiquitinylation of EG5 (Drosopoulos et al., 2014; Eguren et al., 2014). Given the specific activation of the APC/C-CDH1 during mitosis, and given

the relatively low expression and small effect of *Fbxo30* deficiency on EG5 levels at M phase, we suggest that *Fbxo30* and APC/C-CDH1 may function at different phases of the cell cycle in regulating EG5 levels, although the possibility that the different E3 may function in different cell types cannot be ruled out.

The mitotic spindle defects observed in the *Fbxo30*^{-/-} mammary epithelial cells is a direct consequence of Eg5 overexpression, as it can be normalized by shRNA silencing of EG5. Moreover, since normalization of Eg5 activity by monastrol and/or *Kif11* shRNA rescued defects in centrosome homeostasis, cellular proliferation, mammosphere formation, and mammoipoiesis, the defective regulation of EG5 levels is likely the root cause of genome instability and defective mammoipoiesis in the *Fbxo30*^{-/-} mice.

Apart from a critical function of *Fbxo30* in mammoipoiesis described herein, a recent report suggested that *Fbxo30* was negatively regulated by the BMP-signaling pathway and contributed to loss of muscle mass caused by defective BMP signaling (Sartori et al., 2013). However, the *Fbxo30* substrate involved in the regulation of muscle mass was not identified. Paradoxically, mice lacking *Fbxo30* have normal development, fertility, and lifespan. Since the developmental pathway for mammary gland is similar to that of T cell differentiation (Watson and Khaled, 2008), we investigated the possible role of EG5 in the development and accumulation of T cells in the thymus and spleen. We found that cellular compositions of spleen and thymus were largely unaffected by *Fbxo30* deletion (Figures S4 and S5). As a potential explanation for lack of function of *Fbxo30* in spleen cells, we found that expression of *Fbxo30* among spleen cells was considerably lower than in the mammary epithelial cells (Figure S6A). Correspondingly, the levels of EG5 were largely unaffected by deletion of the *Fbxo30* gene (Figure S6B). With recent identification of APC/C-CDH1 as an E3 ligase for EG5 (Drosopoulos et al., 2014; Eguren et al., 2014), it is possible that this or another E3 may serve to regulate EG5 depending on the cell types studied.

Accumulating data have demonstrated that some of the most critical regulators of centrosome homeostasis, including *Plk4*, *SAS6*, and *Cp110*, are regulated by SCF-type E3 ligase (Silverman et al., 2012). Our data demonstrate that Eg5 abundance, as well as its oscillation during cell cycle, also is regulated by an E3 ligase. It is of note that Eg5 levels frequently are elevated in human cancer and that such elevation correlates with poor prognosis (Ding et al., 2011; Saijo et al., 2006). Since transgenic expression of Eg5 leads to abnormal centrosome homeostasis, genetic instability, and cancer development (Castillo et al., 2007), it would be of interest to test whether *Fbxo30* defects may contribute to Eg5 elevation in human cancer.

EXPERIMENTAL PROCEDURES

Generation of *Fbxo30*^{-/-} Mice

The mice were generated by inGenious Targeting Laboratories through a research contract. The constructs generated are diagrammed in Figure S1. Briefly, a 13.2-kb region used to construct the targeting vector was first subcloned from a positively identified B6 BAC clone using a homologous recombination-based technique. The region was designed such that the short homology arm (SA) extended 1.9 kb to the 5' Neo cassette. The long homology arm (LA) started at the 5' end of the GFP cassette and was 7.8 kb. The GFP/Neo cassette was inserted 3 bp before the ATG of exon 1 and replaced ~3.5 kb of the gene sequence. The targeting vector was confirmed by restriction analysis after each modification step and by sequencing using primers designed to read from the LacZ/Neo cassette into the 5' end of the SA (N1) and the 3' end of the LA (GFP1) or from primers that anneal to the vector sequence, P6 and T7, and read into the 5' and 3' ends of the BAC subclone. The BAC was subcloned into a ~2.4-kb backbone vector containing an ampicillin selection cassette for

retransformation of the construct prior to electroporation. The total size of the targeting construct (including vector backbone and GFP/Neo cassette) was 14.7 kb. The targeting vector (10 µg) was linearized by *Ascl* and then transfected by electroporation of iTL C57 BL/6 ESCs. After selection in G418, surviving clones were expanded for PCR analysis to identify recombinant ESC clones. Primers, A1 was designed downstream (3') to the SA outside the region used to generate the targeting construct. ESCs with a targeted locus were injected into albino C57BL/6 blastocysts to generate chimeric mice. Chimera were identified by coat color and used to generate mice with germline transmission of the targeted *Fbxo30*^{-/-} locus.

Generation of HCT116 Cell Line with FLAG-Tagged Endogenous *Fbxo30*

The vector construction and knockin by homologous recombination were based on a previous report (Zhang et al., 2008). Briefly, the targeting vector was constructed by PCR using genomic DNA as the template for the homologous left arm. Homologous recombination was screened by PCR with primers derived from the neomycin resistance gene and the upstream region of the left homologous arm. Two clones were identified from two 96-well plates of G418-resistant clones. The neomycin resistance gene was excised by Cre recombinase. The following primers were used: 3FLAG KI *FBXO30* left arm F, GGGAAG/ideoxyU/atttgaagaatgaggggcttg; 3FLAG KI *FBXO30* left arm R, GGAGACA/ideoxyU/GcAAGTACAGGTTTTAAAACACTGAGCG; 3FLAG KI *FBXO30* right arm F, GGTCCCA/ideoxyU/AAGTTGTAATATTACTAGCACATA; 3FLAG KI *FBXO30* right arm R, GGCATAG/ideoxyU/ACTTCTTGGTGGTGAAGCCTA; 3FLAG KI *FBXO30* left screening F, tctaggtctgctcctgctctgc; 3FLAG KI *FBXO30* right screening R, ttttaagcagaccacatcagg; 3FLAG KI *FBXO30* cre F, GAAGGACGTTCACTACGCTCA; and 3FLAG KI *FBXO30* Cre R, TTCCAAAATTTACACATTTCA.

Immunofluorescence

After deparaffinization and rehydration of slides with Xylene and ethanol, the mammary gland sections from *Fbxo30* knockout and WT mice were treated with 10 mM sodium citrate buffer (pH 6.0). The sections were permeabilized with 0.3% Triton X-100 in 10 mM Tris-HCl buffer for 30 min. After blocking with 2% BSA for 60 min, sections were incubated with primary antibody diluted in 10 mM Tris-HCl buffer containing 2% BSA at 4°C overnight, with subsequent staining with secondary antibody in BSA-Tris-HCl buffer at room temperature for 2–4 hr. The nuclei were stained with DAPI. Slides were mounted with Prolong Antifade mounting buffer (Invitrogen). Antibodies for EG5 (NB500-181, Novus), β-tubulin (F2043, Sigma), γ-tubulin (T5326, Sigma), Keratin 5 (AF138, Covance), Keratin 8 (TROMA-I, Developmental Studies Hybridoma Bank [DSHB]), Keratin K14 (ab7800, Abcam), Keratin K17 (ab53707, Abcam), and αSMA (ab5694, Abcam) were used for immunofluorescence.

Transplantation

Female mice (3 weeks old) were anesthetized with Ketamine and Xylazine. An inverted Y incision was made from the midline point between the fourth set of nipples and ending at a point between the fourth and fifth sets. The fourth and fifth fat pads on each side were exposed using forceps to separate the skin from the body cavity. Half of the fourth mammary fat pad from the fourth nipple to the lymph node was removed using scissors to clear the mammary epithelium, and 1 × 10⁶ mammary epithelial cells suspended in 30 µl Hank's balanced salt solution plus 2% fetal bovine serum (FBS) were injected into the mammary epithelium-cleared fat pads. After cell transplantation, the incision was sutured with 9-mm autoclips, and the mice were placed in a clean cage and were monitored for a short period of time. Staples were removed 2 weeks after surgery.

Isolation and Culture of Mammary Gland Epithelia

Mammary glands were minced with razor blades on a sterile surface and then transferred to a tube containing dissociation solution (EpiCult-B medium with collagenase and Hyaluronidase, STEMCELL Technologies) and incubated for 7 hr at 37°C with occasional pipetting and vortexing. After dissociation, the cells were collected by centrifugation at 350 × g. Pre-warmed Trypsin-EDTA (1–5 ml) was added to the partially dissociated tissue and mixed by pipetting for 1 to 3 min. Cold Hank's balanced salt solution (10 ml) supplemented with

2% FBS was added to stop the digestion, and the cells were again collected by centrifugation at $350 \times g$ for 5 min. To dissociate the clumps, 2 ml pre-warmed 5 mg/ml Dispase (07913, STEMCELL Technologies) and 200 μ l 1 mg/ml DNase I (07900, STEMCELL Technologies) were added to the pellet and then pipetted for 1 min with a P1000 micropipettor to further dissociate cell clumps. The cell suspension was then diluted with an additional 10 ml cold Hank's balanced salt solution supplemented with 2% FBS and filtered through a 40- μ m cell strainer into a new 50-ml centrifuge tube. Cells were collected after centrifugation and red blood cells were lysed as needed.

Flow Cytometry

The isolated cells from the mammary glands of WT and *Fbxo30*^{-/-} mice were stained with fluorochrome-conjugated anti-CD31, CD45.2, CD61, CD24, CD49f, CD29, Sca-1, and CD133 monoclonal antibodies (eBioscience). The stained cells were analyzed by a fluorescence-activated cell analyzer (LSR II).

Mammosphere Assay

The isolated cells from the mammary glands of either WT or *Fbxo30*^{-/-} mice were suspended in the EpiCult-B (STEMCELL Technologies) and seeded in ultra-low attachment six-well plates (Corning). The cells were cultured for 7 days and the formed mammospheres were photographed. The surface areas of the mammospheres were measured based on analysis of the images using Scion image software.

Whole-Mount Staining

Whole-mount preparations of mammary glands were performed according to the protocol reported by Mueller et al. (2002). Briefly, inguinal number 4 mammary glands were dissected, spread on glass slides, and fixed overnight in Carnoy's fixative. The next day, the tissues were hydrated and then stained in carmine-aluminum stain overnight. The tissues were dehydrated, cleared in xylene, and mounted between two glass slides using Permount mounting media.

shRNA Silencing

The lentiviral vector pLenti6/V5-TOPO, obtained from Invitrogen, was modified by replacing the CMV promoter with a U6 promoter to drive an shRNA-expressing cassette and inserting a pGK-driven EGFP cassette and a blasticidin-resistant cassette. The sequence used to silence *Kif11* was 5'-TGCAGGT CAGATTACTACT-3' (sh1) and TATTGCTTCAGGCTCTCA (sh2). The MGE cell cultures were infected with either scrambled shRNA control lentivirus or lentivirus encoding *Kif11*-shRNA for 24 hr. After recovery for an additional 48 hr, the cultures were used for assays.

In Vitro Ubiquitinylation Assay

All the reagents used for the in vitro ubiquitinylation assay were purchased from Boston Biochem (K930). Ubiquitinylation was performed according to standard protocols provided by the supplier, with modifications. In brief, HEK293 cells were transfected with Eg5-Myc or its phosphorylation site mutants. Anti-Myc immunoprecipitate beads were mixed with components of the ubiquitinylation system in the presence or absence of Fbxo30 proteins, which were eluted using FLAG peptide from anti-FLAG immunoprecipitates of transfected HEK293 cells using FLAG peptide. After 2 hr of incubation at 37°C, the beads were washed with a 1% Triton X-100 Tris-HCl buffer, resuspended with a 2% SDS Tris-HCl buffer, and re-immunoprecipitated with an anti-Myc antibody after a 10-fold dilution with a 1% Triton X-100 Tris-HCl buffer. The final immunoprecipitates were resuspended in SDS loading buffer, heated for 3 min at 90°C, and resolved by 10% SDS-PAGE.

Immunoprecipitation and Western Blot

Cells or tissues were lysed with a 1% Triton X-100 buffer containing 20 mM Tris-HCl (pH 7.4), 150 mM NaCl, 40 mM NaF, 2 mM DTT, and a protease and phosphatase inhibitor cocktail (Sigma). The cleared lysates were immunoprecipitated with protein G beads and antibody at 4°C with overnight shaking. After washing with the lysis buffer for three times, the beads were treated with SDS loading buffer and the eluted proteins were analyzed by western blot. The EG5 antibodies used for western blot and immunoprecipitation were a rabbit antibody (ab61199, Abcam) and a mouse antibody (NB100-78467, Novus Biologicals), respectively.

Measurement of Duct and Branch Lengths

The ratio of branch over duct length was measured using a method developed for measuring neurite and axon lengths (Kim et al., 2013; Sterne et al., 2015). The NeuroLucida software (MBF Bioscience) was used to trace and measure the length of duct and that of the branches in a double-blind fashion. Total lengths of either ducts or branches in all areas captured in low-power images (see Figures 1A, 1B, and 6D as examples) were integrated to calculate the branch over duct ratios.

Statistics

Student's t test was used to determine statistical significance between two groups of samples.

SUPPLEMENTAL INFORMATION

Supplemental Information includes six figures and one table can be found with this article online at <http://dx.doi.org/10.1016/j.celrep.2016.03.083>.

AUTHOR CONTRIBUTIONS

Yan Liu and Y.W. performed the experiments. Yang Liu, P.Z., and Y.W. supervised the study. Yan Liu, Y.W., P.Z., and Yang Liu prepared the manuscript. Z.D. and X.Y. generated the FDX3-FLAG tag knockin cell line.

ACKNOWLEDGMENTS

We thank Dr. Jane Visvader and Bing Ye for valuable advice; Drs. Junlin Guan, Yuan Zhu, and Kaoru Sakebe for critical reading of the manuscript; and Ms. Morgan Daley for editing the manuscript. This study was supported by grants from the NIH and the U.S. Department of Defense.

Received: July 31, 2015

Revised: February 17, 2016

Accepted: March 23, 2016

Published: April 21, 2016

REFERENCES

- Asselin-Labat, M.L., Sutherland, K.D., Barker, H., Thomas, R., Shackleton, M., Forrest, N.C., Hartley, L., Robb, L., Grosveld, F.G., van der Wees, J., et al. (2007). Gata-3 is an essential regulator of mammary-gland morphogenesis and luminal-cell differentiation. *Nat. Cell Biol.* 9, 201–209.
- Bertran, M.T., Sdelci, S., Regué, L., Avruch, J., Caelles, C., and Roig, J. (2011). Nek9 is a Plk1-activated kinase that controls early centrosome separation through Nek6/7 and Eg5. *EMBO J.* 30, 2634–2647.
- Blangy, A., Lane, H.A., d'Hérin, P., Harper, M., Kress, M., and Nigg, E.A. (1995). Phosphorylation by p34cdc2 regulates spindle association of human Eg5, a kinesin-related motor essential for bipolar spindle formation in vivo. *Cell* 83, 1159–1169.
- Bouras, T., Pal, B., Vaillant, F., Harburg, G., Asselin-Labat, M.L., Oakes, S.R., Lindeman, G.J., and Visvader, J.E. (2008). Notch signaling regulates mammary stem cell function and luminal cell-fate commitment. *Cell Stem Cell* 3, 429–441.
- Carrano, A.C., Eytan, E., Hershko, A., and Pagano, M. (1999). SKP2 is required for ubiquitin-mediated degradation of the CDK inhibitor p27. *Nat. Cell Biol.* 1, 193–199.
- Castillo, A., Morse, H.C., 3rd, Godfrey, V.L., Naeem, R., and Justice, M.J. (2007). Overexpression of Eg5 causes genomic instability and tumor formation in mice. *Cancer Res.* 67, 10138–10147.
- Chakrabarti, R., Wei, Y., Romano, R.A., DeCoste, C., Kang, Y., and Sinha, S. (2012). E1f5 regulates mammary gland stem/progenitor cell fate by influencing notch signaling. *Stem Cells* 30, 1496–1508.
- D'Angioletti, V., Donato, V., Vijayakumar, S., Saraf, A., Florens, L., Washburn, M.P., Dynlacht, B., and Pagano, M. (2010). SCF(Cyclin F) controls centrosome

- homeostasis and mitotic fidelity through CP110 degradation. *Nature* 466, 138–142.
- D'Angiolella, V., Donato, V., Forrester, F.M., Jeong, Y.T., Pellacani, C., Kudo, Y., Saraf, A., Florens, L., Washburn, M.P., and Pagano, M. (2012). Cyclin F-mediated degradation of ribonucleotide reductase M2 controls genome integrity and DNA repair. *Cell* 149, 1023–1034.
- Ding, S., Xing, N., Lu, J., Zhang, H., Nishizawa, K., Liu, S., Yuan, X., Qin, Y., Liu, Y., Ogawa, O., and Nishiyama, H. (2011). Overexpression of Eg5 predicts unfavorable prognosis in non-muscle invasive bladder urothelial carcinoma. *Int. J. Urol.* 18, 432–438.
- Drosopoulos, K., Tang, C., Chao, W.C., and Linardopoulos, S. (2014). APC/C is an essential regulator of centrosome clustering. *Nat. Commun.* 5, 3686.
- Duan, S., Cermak, L., Pagan, J.K., Rossi, M., Martinengo, C., di Celle, P.F., Chapuy, B., Shipp, M., Chiarle, R., and Pagano, M. (2012). FBXO11 targets BCL6 for degradation and is inactivated in diffuse large B-cell lymphomas. *Nature* 481, 90–93.
- Eguren, M., Álvarez-Fernández, M., García, F., López-Contreras, A.J., Fujimitsu, K., Yaguchi, H., Luque-García, J.L., Fernández-Capetillo, O., Muñoz, J., Yamano, H., and Malumbres, M. (2014). A synthetic lethal interaction between APC/C and topoisomerase poisons uncovered by proteomic screens. *Cell Rep.* 6, 670–683.
- Frescas, D., and Pagano, M. (2008). Deregulated proteolysis by the F-box proteins SKP2 and beta-TrCP: tipping the scales of cancer. *Nat. Rev. Cancer* 8, 438–449.
- Ganem, N.J., Godinho, S.A., and Pellman, D. (2009). A mechanism linking extra centrosomes to chromosomal instability. *Nature* 460, 278–282.
- Guo, W., Keckesova, Z., Donaher, J.L., Shibue, T., Tischler, V., Reinhardt, F., Itzkovitz, S., Noske, A., Zürer-Härdi, U., Bell, G., et al. (2012). Slug and Sox9 cooperatively determine the mammary stem cell state. *Cell* 148, 1015–1028.
- Jin, J., Cardozo, T., Lovering, R.C., Elledge, S.J., Pagano, M., and Harper, J.W. (2004). Systematic analysis and nomenclature of mammalian F-box proteins. *Genes Dev.* 18, 2573–2580.
- Kim, J.H., Wang, X., Coolon, R., and Ye, B. (2013). Dscam expression levels determine presynaptic arbor sizes in *Drosophila* sensory neurons. *Neuron* 78, 827–838.
- Kõivomägi, M., Valk, E., Venta, R., Iofik, A., Lepiku, M., Balog, E.R., Rubin, S.M., Morgan, D.O., and Loog, M. (2011). Cascades of multisite phosphorylation control Sic1 destruction at the onset of S phase. *Nature* 480, 128–131.
- Kuchay, S., Duan, S., Schenkein, E., Peschiaroli, A., Saraf, A., Florens, L., Washburn, M.P., and Pagano, M. (2013). FBXL2- and PTPL1-mediated degradation of p110-free p85 β regulatory subunit controls the PI(3)K signalling cascade. *Nat. Cell Biol.* 15, 472–480.
- Liu, C., Li, Y., Semenov, M., Han, C., Baeg, G.H., Tan, Y., Zhang, Z., Lin, X., and He, X. (2002). Control of beta-catenin phosphorylation/degradation by a dual-kinase mechanism. *Cell* 108, 837–847.
- Mardin, B.R., and Schiebel, E. (2012). Breaking the ties that bind: new advances in centrosome biology. *J. Cell Biol.* 197, 11–18.
- Mardin, B.R., Agircan, F.G., Lange, C., and Schiebel, E. (2011). Plk1 controls the Nek2A-PP1 γ antagonism in centrosome disjunction. *Curr. Biol.* 21, 1145–1151.
- Mayer, T.U., Kapoor, T.M., Haggarty, S.J., King, R.W., Schreiber, S.L., and Mitchison, T.J. (1999). Small molecule inhibitor of mitotic spindle bipolarity identified in a phenotype-based screen. *Science* 286, 971–974.
- Mueller, S.O., Clark, J.A., Myers, P.H., and Korach, K.S. (2002). Mammary gland development in adult mice requires epithelial and stromal estrogen receptor alpha. *Endocrinology* 143, 2357–2365.
- Nash, P., Tang, X., Orlicky, S., Chen, Q., Gertler, F.B., Mendenhall, M.D., Sicheri, F., Pawson, T., and Tyers, M. (2001). Multisite phosphorylation of a CDK inhibitor sets a threshold for the onset of DNA replication. *Nature* 414, 514–521.
- Nigg, E.A., and Stearns, T. (2011). The centrosome cycle: Centriole biogenesis, duplication and inherent asymmetries. *Nat. Cell Biol.* 13, 1154–1160.
- Oakes, S.R., Naylor, M.J., Asselin-Labat, M.L., Blazek, K.D., Gardiner-Garden, M., Hilton, H.N., Kazlauskas, M., Pritchard, M.A., Chodosh, L.A., Pfeffer, P.L., et al. (2008). The Ets transcription factor Elf5 specifies mammary alveolar cell fate. *Genes Dev.* 22, 581–586.
- Puklowski, A., Homsy, Y., Keller, D., May, M., Chauhan, S., Kossatz, U., Grünwald, V., Kubicka, S., Pich, A., Manns, M.P., et al. (2011). The SCF-FBXW5 E3-ubiquitin ligase is regulated by PLK4 and targets HsSAS-6 to control centrosome duplication. *Nat. Cell Biol.* 13, 1004–1009.
- Raouf, A., Zhao, Y., To, K., Stingl, J., Delaney, A., Barbara, M., Iscove, N., Jones, S., McKinney, S., Emerman, J., et al. (2008). Transcriptome analysis of the normal human mammary cell commitment and differentiation process. *Cell Stem Cell* 3, 109–118.
- Rapley, J., Nicolàs, M., Groen, A., Regué, L., Bertran, M.T., Caelles, C., Avruch, J., and Roig, J. (2008). The NIMA-family kinase Nek6 phosphorylates the kinesin Eg5 at a novel site necessary for mitotic spindle formation. *J. Cell Sci.* 121, 3912–3921.
- Saijo, T., Ishii, G., Ochiai, A., Yoh, K., Goto, K., Nagai, K., Kato, H., Nishiwaki, Y., and Saijo, N. (2006). Eg5 expression is closely correlated with the response of advanced non-small cell lung cancer to antimitotic agents combined with platinum chemotherapy. *Lung Cancer* 54, 217–225.
- Sartori, R., Schirwis, E., Blaauw, B., Bortolanza, S., Zhao, J., Enzo, E., Stantzu, A., Mouisel, E., Toniolo, L., Ferry, A., et al. (2013). BMP signaling controls muscle mass. *Nat. Genet.* 45, 1309–1318.
- Shackleton, M., Vaillant, F., Simpson, K.J., Stingl, J., Smyth, G.K., Asselin-Labat, M.L., Wu, L., Lindeman, G.J., and Visvader, J.E. (2006). Generation of a functional mammary gland from a single stem cell. *Nature* 439, 84–88.
- Silverman, J.S., Skaar, J.R., and Pagano, M. (2012). SCF ubiquitin ligases in the maintenance of genome stability. *Trends Biochem. Sci.* 37, 66–73.
- Skaar, J.R., Pagan, J.K., and Pagano, M. (2013). Mechanisms and function of substrate recruitment by F-box proteins. *Nat. Rev. Mol. Cell Biol.* 14, 369–381.
- Sterne, G.R., Kim, J.H., and Ye, B. (2015). Dysregulated Dscam levels act through Abelson tyrosine kinase to enlarge presynaptic arbors. *eLife* 4, e05196.
- Stingl, J., Eirew, P., Ricketson, I., Shackleton, M., Vaillant, F., Choi, D., Li, H.I., and Eaves, C.J. (2006). Purification and unique properties of mammary epithelial stem cells. *Nature* 439, 993–997.
- Visvader, J.E. (2009). Keeping abreast of the mammary epithelial hierarchy and breast tumorigenesis. *Genes Dev.* 23, 2563–2577.
- Visvader, J.E., and Stingl, J. (2014). Mammary stem cells and the differentiation hierarchy: current status and perspectives. *Genes Dev.* 28, 1143–1158.
- Watson, C.J., and Khaled, W.T. (2008). Mammary development in the embryo and adult: a journey of morphogenesis and commitment. *Development* 135, 995–1003.
- Wei, W., Jin, J., Schlisio, S., Harper, J.W., and Kaelin, W.G., Jr. (2005). The v-Jun point mutation allows c-Jun to escape GSK3-dependent recognition and destruction by the Fbw7 ubiquitin ligase. *Cancer Cell* 8, 25–33.
- Yalcin-Ozuysal, O., Fiche, M., Gutierrez, M., Wagner, K.U., Raffoul, W., and Briskin, C. (2010). Antagonistic roles of Notch and p63 in controlling mammary epithelial cell fates. *Cell Death Differ.* 17, 1600–1612.
- Yoshida, Y., Chiba, T., Tokunaga, F., Kawasaki, H., Iwai, K., Suzuki, T., Ito, Y., Matsuoka, K., Yoshida, M., Tanaka, K., and Tai, T. (2002). E3 ubiquitin ligase that recognizes sugar chains. *Nature* 418, 438–442.
- Zhang, X., Guo, C., Chen, Y., Shulha, H.P., Schnetz, M.P., LaFramboise, T., Bartels, C.F., Markowitz, S., Weng, Z., Scacheri, P.C., and Wang, Z. (2008). Epitope tagging of endogenous proteins for genome-wide ChIP-chip studies. *Nat. Methods* 5, 163–165.